7 The $Fe(CN)_6^{3-}$ / $Fe(CN)_6^{4-}$ charge transfer reaction on Au(111) revisited in the presence and absence of a two-dimensional condensed organic film

7.1 Introduction

As reported in chapter 4, the $Fe(CN)_6^{3-}/Fe(CN)_6^{4-}$ redox reaction was originally considered to be a promising candidate for the Turing structure experiments because it is routinely used to probe the extent of the inhibition of the electron transfer by an organic monomolecular film. These studies are based on the assumption that the $Fe(CN)_6^{3-/4-}$ redox reaction is a simple, reversible electron transfer reaction. However, already after a few SPRA experiments it was apparent that the charge-transfer kinetics of the $Fe(CN)_6^{3-}/Fe(CN)_6^{4-}$ reaction at the camphor/Au interface deviates considerably from this picture. Moreover, there are also a few indications in literature that the $Fe(CN)_6^{3-}/Fe(CN)_6^{4-}$ reaction might cause some destruction of an organic film [100]. It is also known that the $Fe(CN)_6^{3-}/Fe(CN)_6^{4-}$ on bare Au electrodes sensitively depends on the composition and concentration of the electrolyte, and under some conditions the formation of adsorbates was found [101-105]. However, despite extensive studies there is still some dispute over whether there is some adsorption of a hexacyanoferrate species [106] as well as over the nature of the adsorbate, which was discussed to be either one or both of the redox species $Fe(CN)_6^{3-/4-}$ [107, 108] itself or a more complex 'reaction product' formed from these species [103, 109-113].

Because of the importance of this reaction and the fact that SP measurements allow to monitor the coverage of the electrode very sensitively, the hexacyanoferrate(III)(ferricyanide) / hexacyanoferrate(II)(ferrocyanide) redox reaction was studied in more detail in the presence and absence of camphor. These studies on the $Fe(CN)_6^{3-}/Fe(CN)_6^{4-}$ (camphor/) Au film electrode system

were done in close collaboration with Julia Oslonovitch, who carried out cyclic voltammetric studies as well as capacitance measurements with identical electrolytes but rotating Au(111) electrodes. The respective sets of experiments are supplementary, and a complete picture of the processes occurring at the interface can only be obtained by considering the single crystal and the film experiments together. The compilation of all the results and their interpretation is the topic of this chapter.

7.2 Inhibition of the $Fe(CN)_6^{3-/4-}$ charge transfer reaction through the camphor film at negative electrode potentials

Results

In chapters 4 and 5 it was discussed that camphor forms a condensed, physisorbed film on the electrode surface in the potential region between about -1.0 V and 0.2 V. When using $Fe(CN)_6^{3-}$ or $Fe(CN)_6^{4-}$ as electroactive species, the influence of the camphor film on the electron transfer rate (etr) turned out to depend strongly on the most positive turning point in the potentio-dynamic experiments. First, consider the CVs obtained when restricting the potential region to values negative of -0.3 V. The solid curve in Fig. 7.1a shows a CV of a rotating Au(111) electrode in an electrolyte containing 0.8 M $NaClO_4$, 0.2 mM $Fe(CN)_6^{3-}$, and 5 mM camphor. For comparison, also the CV in the same solution but without camphor is displayed (dashed curve). The peak pair slightly negative to -0.6 V stems from the adsorption of camphor; its existence suggests strongly that the phase transition takes place also in the presence of $Fe(CN)_6^{3-}$ under the chosen experimental conditions. Around the phase transition, the reduction rate of $Fe(CN)_6^{3-}$ has already attained a mass transport limited value and the current density is not noticeably affected by the formation or dissolution of the camphor film.

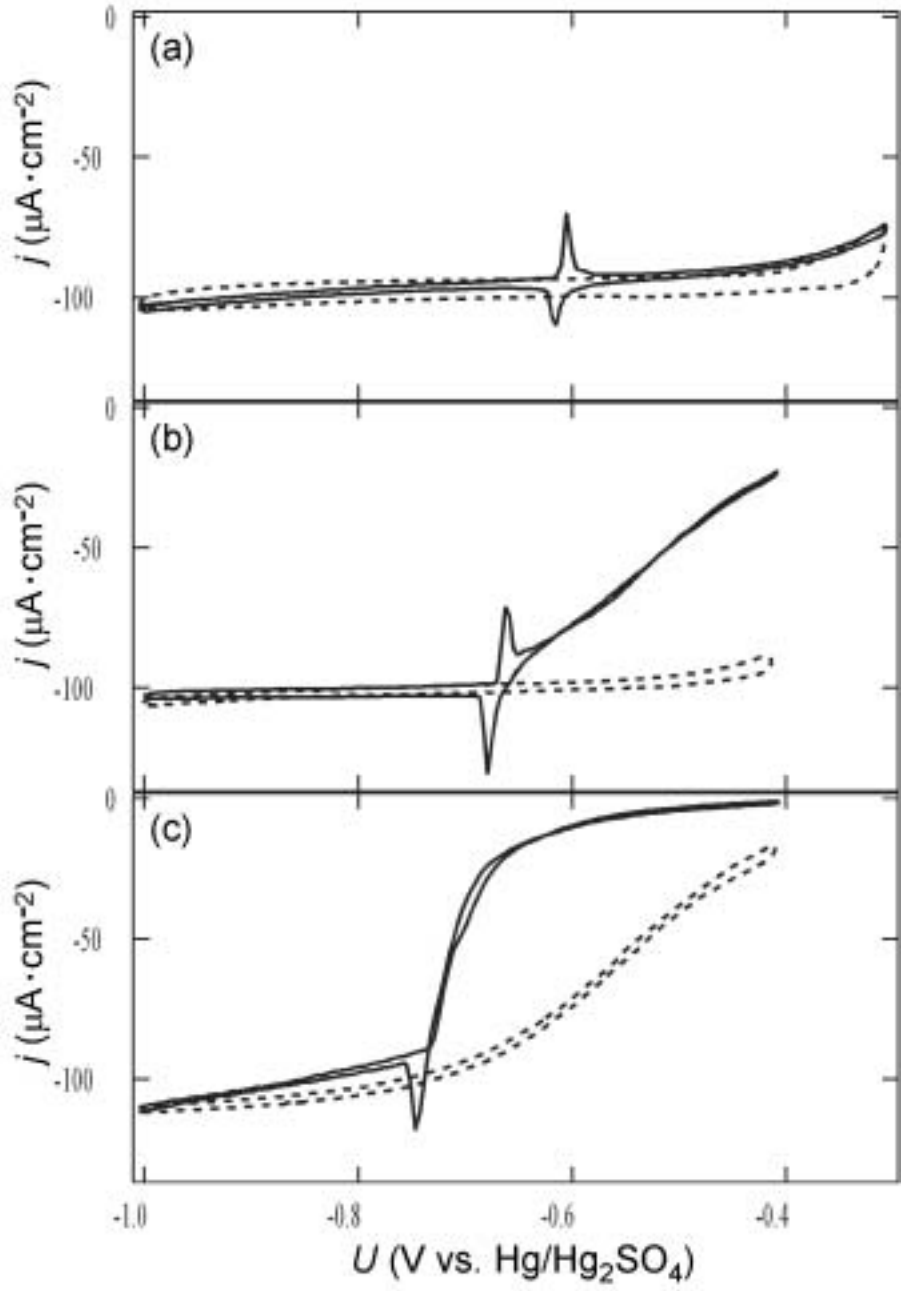

Figure 7.1: *Influence of the camphor film on hexacyanoferrate(III) reduction on Au(111) for different perchlorate concentrations in the cathodic potential region: a) 0.8 M, b) 0.1 M, and c) 0.02 M $NaClO_4$. (Electrolyte: 0.2 mM $K_3[Fe(CN)_6]$, 0.8 or 0.1 or 0.2 mM $NaClO_4$, and 5 mM camphor (solid curves); dashed curves: without camphor; rotation frequency 28 rps; scan rate 50 mV/s).*

The picture changes at lower concentration of the base electrolyte. The CVs in Figs. 7.1b and 7.1c were obtained in solutions containing 0.1 M and 0.02 M $NaClO_4$, respectively. Again, the solid curves were recorded in camphor containing solutions and the dashed curves without camphor. In both cases it is evident that $Fe(CN)_6^{3-}$ reduction is considerably inhibited by the presence of the film. However, the inhibition is not complete. Furthermore, the reaction current at a given potential is clearly significantly larger in the 0.1 M than in the 0.02 M $NaClO_4$ solution. Note that the concentration of the supporting electrolyte has also a considerable effect on the existence range, and thus the stability of the camphor film. Compared to the 0.8 M $NaClO_4$ base electrolyte, in the 0.02 M solution the phase transition of camphor is shifted by approximately 150 mV into the negative direction, for the 0.1 M solution it occurs at an intermediate value.

It is well established that also in the absence of a surfactant the rate of $Fe(CN)_6^{3-}$ reduction depends on the concentration of the supporting electrolyte (see, e.g., [105] and refs. therein), the reaction being more irreversible for lower electrolyte conductivity. In Fig. 7.1b, i.e., in a 0.1 M perchlorate solution, the reaction rate is in a mass transfer dominated regime in the whole potential range shown such that the decrease in the reaction rate compared to the 0.8 M solution is not apparent in these experiments. In contrast, in the 0.02 M solution the more irreversible character of $Fe(CN)_6^{3-}$ reduction is clearly discernible.

The irreversibility of $Fe(CN)_6^{3-}$ reduction in diluted electrolyte solutions can be lifted by adding small amounts of a salt with a multiply charged cation, such as Ba^{2+}, Ca^{2+}, La^{3+} or Th^{4+} [104, 105]. Adding a small amount of $Ba(ClO_4)_2$ to a camphor containing diluted electrolyte changes also the reaction current in the presence of the camphor film considerably. This can be seen in Fig. 7.2 where the current–voltage characteristics of $Fe(CN)_6^{3-}$ reduction on the Au(111)/camphor electrode in 0.02 M $NaClO_4$ solution before (dashed) and after the addition of Ba^{2+} ions are reproduced.

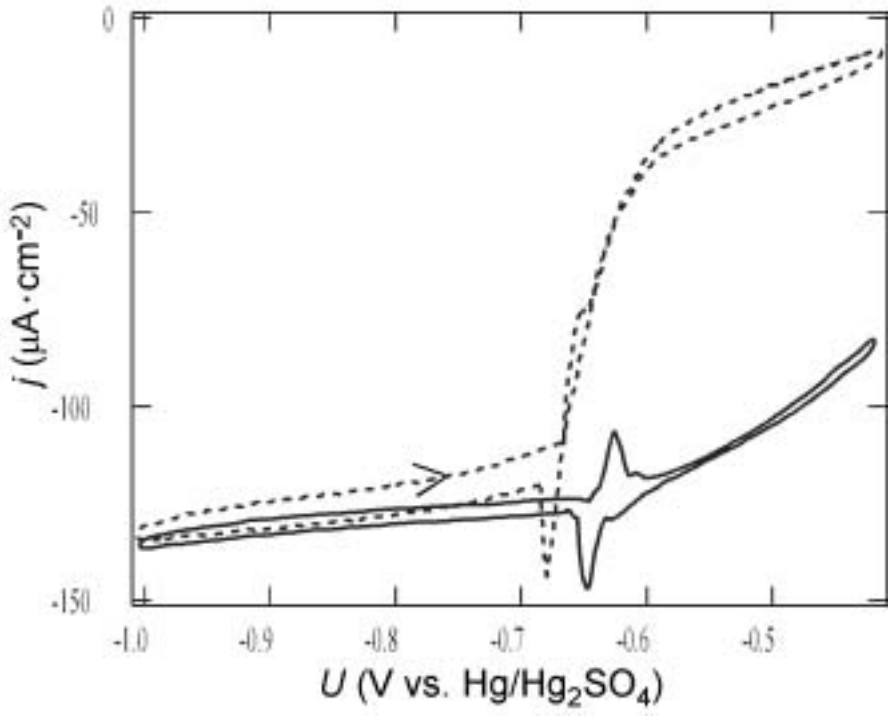

Figure 7.2: *Cyclic voltammograms of a rotating Au(111) electrode in 5 mM camphor, 0.2 mM $K_3[Fe(CN)_6]$, 0.2 mM $K_4[Fe(CN)_6]$, 20 mM $NaClO_4$ (dashed line), and in the same electrolyte after addition of 2 mM $Ba(ClO_4)_2$ (solid line). (Rotation frequency 28 rps, scan rate 50 mV/s).*

Discussion

The results presented thus far clearly show that a) the formation of the condensed camphor film occurs also in the presence of $Fe(CN)_6^{3-/4-}$ if the potential is kept negative to -0.3 V and b) that at least at low ionic strength the redox reaction rate is slowed down due to the presence of the condensed film. It is not the objective here to quantitatively evaluate the effect of the camphor film on the rate constant of the electron transfer reaction. However, it seems to be worthwhile to roughly estimate the influence of the condensed film.

The reaction current density of a simple electron transfer reaction (neglecting double layer effects) at a rotating disc electrode as a function of the overpotential η is given by [114]:

$$\frac{1}{j(\eta)} = \frac{1}{j_D(\mu)}\left\{1 + \left(\frac{k^+ A_{red}}{D_{red}} + \frac{k^- A_{ox}}{D_{ox}}\right)\frac{1}{\sqrt{\omega}}\right\} \qquad (7.1)$$

with

$j_D = nF\left(k^+ c^0_{red} - k^- c^0_{ox}\right)$, $k^+ = k^+_0 \exp\left(\alpha nF\eta / RT\right)$,

$k^- = k^-_0 \exp\left(-(1-\alpha)nF\eta / RT\right)$, and $A_{red(ox)} = 1{,}61\nu^{1/6} D_{red(ox)}{}^{1/3}$,

where ω is the rotation frequency, $k_0^{-(+)}$, $D_{red(ox)}$ are the rate constants and diffusion constant of the reduced (oxidized) species, respectively, and $c^0_{red(ox)}$ their bulk concentrations. ν is the kinematic viscosity and α, n, F, R and T have their usual meanings.

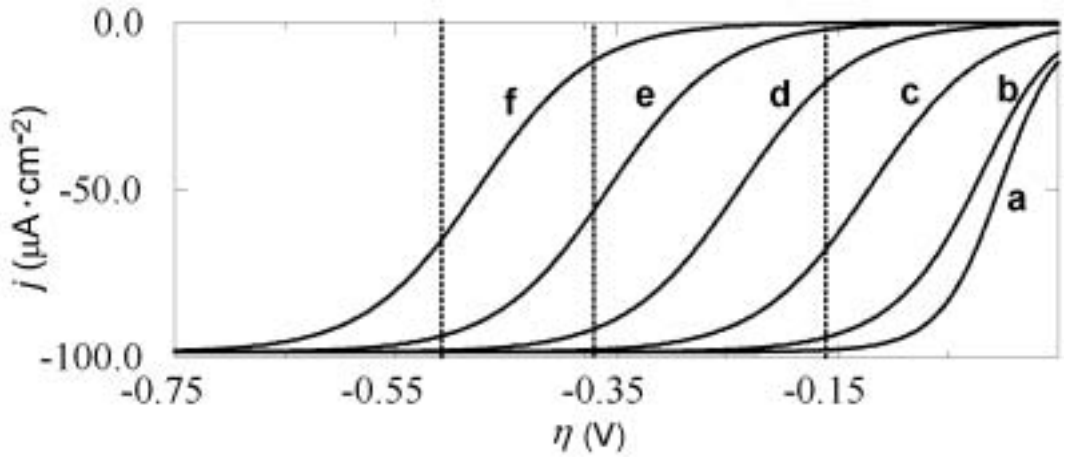

Figure 7.3: *According to Eq. (7.1), calculated current–overpotential curves for different values of* $k_0^{-(+)}$. *From right to left* $k_0^{-(+)}$ *was successively decreased by a factor of 10. The dashed lines indicate the range of overpotential in Fig. 3, in which hexacyanoferrate(III) reduction proceeds on a camphor covered electrode if the formal redox potential is taken to be -0.24 V vs. Hg/Hg₂SO₄ (This was determined in independent experiments, see also Fig. 7).*

Most right curve: $k^-_0 = k^+_0 = 0.05$. Other parameters are:

$c^0_{red} = 0.2\,\text{mM}, c^0_{ox} = 0\,\text{mM}, \left(\alpha nF / RT\right) = \left((1-\alpha)nF / RT\right) = 19.46\,\text{V}^{-1}$,

$D_{red} = D_{ox} = 6 \cdot 10^{-6}\,\text{cm}^2/\text{s}, \nu = 0.01, \omega = 2\pi\,30\,\text{s}^{-1}$.

Fig. 7.3 displays $j(\eta)$ as calculated from Eq. (7.1) as a function of η for different values of $k_0^{-(+)}$ and the other parameters adopted to the experiment of Fig. 7.1.

Curve (a) was obtained for $k_0^- = k_0^+ = 0.05\,\mathrm{cm/s}$, which is reported for the $Fe(CN)_6^{3-/4-}$ redox reaction at Pt in 0.5 M K_2SO_4 [114] and is of the same order of magnitude as the value determined on Au in 0.5 M K_2SO_4 [115]. Hence, curve (a) corresponds roughly to the camphor free system in concentrated base electrolyte (cf. Fig. 7.1a, dashed curve). Curves (b) to (f) result when reducing the rate constants successively by a factor of 10. The vertical lines indicate the potential region between the positive turning point and the potential, at which the phase transitions occur in Figs. 7.1a and 7.1c, respectively, for easier comparison. Assuming that we can neglect the contribution of the reaction current at 'holes' or 'defects' in the camphor film, a comparison between the experimental and calculated current–potential curves of Figs. 7.1 and 7.3 suggests that the camphor film slows down the reaction rate two to three orders of magnitude for the two lower base electrolyte concentrations (Figs. 7.1b and 7.1c) but not more than one order of magnitude in the case of the concentrated supporting electrolyte. Considering the fact that we can roughly estimate the thickness of the camphor layer by 6.6 Å [116], this comparatively small decrease of the reaction rate appears to be reasonable. However, it is remarkable that on Hg [117] a condensed camphor layer was found to inhibit the charge transfer considerably more strongly than we observed it on Au. At present it remains unclear, from where these differences result.

The assumption that the current density at holes can be neglected is the worse, the faster the reaction rate, and thus in our case the worst for the concentrated electrolyte. However, for the parameters of the experiments the current density at defects should still not dominate the current density in the potential regions shown: In Fig. 7.1a and Fig. 7.1b the current on the bare Au electrode just enters the mass transport limited region at the positive turning point (note that in Fig. 7.1a it was chosen 100 mV more positive than in Fig. 7.1b); in Fig. 7.1c the current is in a region of mixed reaction and transport control in the entire potential region of interest. This strongly suggests that the camphor film indeed slows down the reaction rate more effectively at low conductivity than at high conductivity.

The reduction of anions sensitively depends on the double layer structure. Thus, a plausible interpretation of the increased inhibition at low base electrolyte concentration would be that the decreased electron transfer rate results from a change of surface charge and potential due to the adsorption of the camphor layer. This picture is supported by the fact that the addition of multivalent cations has the same effect on the reduction rate of $Fe(CN)_6^{3-}$ in the diluted electrolyte in the presence and absence of camphor (cf. Fig. 7.2). A decrease in the electron transfer rate with decreasing concentration of the base electrolyte was also reported for $S_2O_8^{2-}$ and $Fe(CN)_6^{3-}$ reduction on Hg in the presence of camphor [117], where the same conclusions were derived. However, in experiments with the camphor/IO_4^- system we also obtained evidence that the camphor film is less stable in electrolytes with high ionic strength than in those with low ionic strength. Thus, it is conceivable that at high conductivity the two-dimensional camphor film is more mobile or flexible such that hydrated ions or water can temporarily penetrate the film and facilitate the electron transfer. In this case, there would be two different reaction pathways, electron transfer through the camphor film and electron transfer at the dynamically formed 'holes' in the film which are occupied by electrolyte species. The observed dependence of the reaction rate on the conductivity is most likely a combination of both, double layer effects and the different flexibility of the condensed camphor phase at different base electrolyte conductivity.

7.3 Replacement of the camphor film by a polymeric hexacyanoferrate film at positive potentials

7.3.1 Cyclic voltammetry and capacitance measurements on bulk Au(111) electrodes

Results

Next we consider the properties of the camphor/hexacyanoferrate system at more positive potentials. Fig. 7.4a displays CVs obtained when sweeping the applied voltage between -1 V and 0.2 V in a solution containing 0.1 M $NaClO_4$

and 5 mM $Fe(CN)_6^{3-}$, whereby the solid curves were obtained in a camphor containing solution, the dashed curve in a camphor free electrolyte. Both CVs display hystereses between positive and negative scans which are, at least partly, due to double layer effects. Moreover, the reaction current in the camphor containing system is larger than in the camphor free system on the negative scan, indicating that the extent of adsorption of camphor on the electrode is minimal. This conclusion is also supported by the most striking difference between the CVs displayed here and those displayed in Fig. 7.1, namely that the phase transition peak of the camphor adlayer is absent. Carrying out the reaction under reversible conditions, e.g., in electrolytes containing small amounts of multivalent cations, the CVs in camphor containing and camphor free solutions are practically identical. Such an example is shown in Fig. 7.4b, where the only hint to the presence of camphor is a minor hump in the positive scan at the potential at which camphor alone exhibits a phase transition due to the formation of the condensed layer. Hence, we conclude that when the potential is cycled between -1.0 and + 0.2 V, the formation of the condensed camphor layer does not occur anymore.

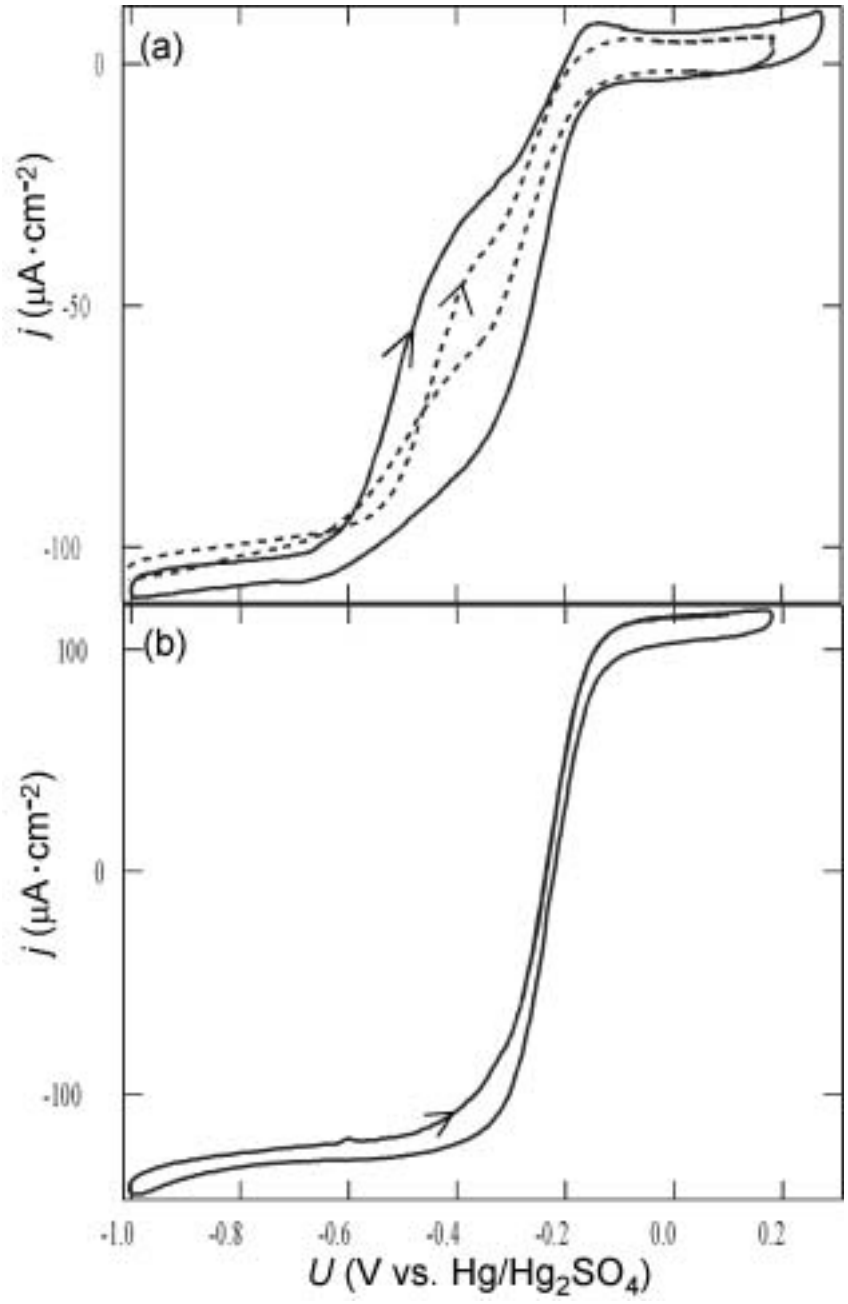

Figure 7.4: *Cyclic voltammograms of the $K_3[Fe(CN)_6]$/ $K_4[Fe(CN)_6]$ redox system on a rotating Au(111) electrode in the potential region from -1.0 to +0.2 V and different electrolytes. (a) 0.2 mM $K_3[Fe(CN)_6]$, 0.1 M $NaClO_4$ with (solid line) and without 5 mM camphor (dashed line); (b) 5 mM camphor, 0.2 mM $K_3[Fe(CN)_6]$, 0.2 mM $K_4[Fe(CN)_6]$, 20 mM $NaClO_4$, 2 mM $Ba(ClO_4)_2$. In (a) and (b) the rotation frequency was 28 rps and the scan rate 50 mV/s.*

More evidence of this qualitative change in behavior is shown in Fig. 7.5, where a series of four cyclic voltammograms of the Au(111)/$Fe(CN)_6^{4-}$, camphor, ClO_4^-

system are depicted together with simultaneously recorded capacitance–voltage curves for different positive turning points, U_p. Since the oxidation current is negligible in the potential range of interest, the capacitance was calculated under the assumption that the double layer behaves like an ideal capacitor. (Note that this implies that the capacitance data are not reliable for U > -0.2 V.) If U_p is chosen negative to -0.3 V, the camphor film forms and dissolves as discussed above. However, when setting U_p to a value positive of -0.2 V, the phase transition peaks disappear in the current–potential curves. As can be seen in the capacitance−voltage plots, in the positive scan some adsorption of camphor still takes place around -0.6 V, which leads in the case of U_p = -0.15 V still to a slight decrease of the capacitance (Fig. 7.5b). For U_p = 0.1 V the amount adsorbed is obviously so small that a decrease of the capacitance is not visible any more (Fig. 7.5c). In the negative voltage scan, the capacitance–voltage curves in Figs. 7.5 b and 7.5c do not exhibit a pseudo-capacitive peak which would arise from desorption of camphor. When restricting U_p again to -0.35 V, the phase transition peaks reappear after some time (Fig. 7.5d). The sharpness of the peaks and the time needed to recover them depended on the time, in which the electrode was cycled to potentials more positive than -0.2 V, as well as on the most positive value of U_p. Obviously, at U > -0.2 V, a process takes place that changes the electrode surface and is not reversible on the time scale of the cyclic voltammogram.

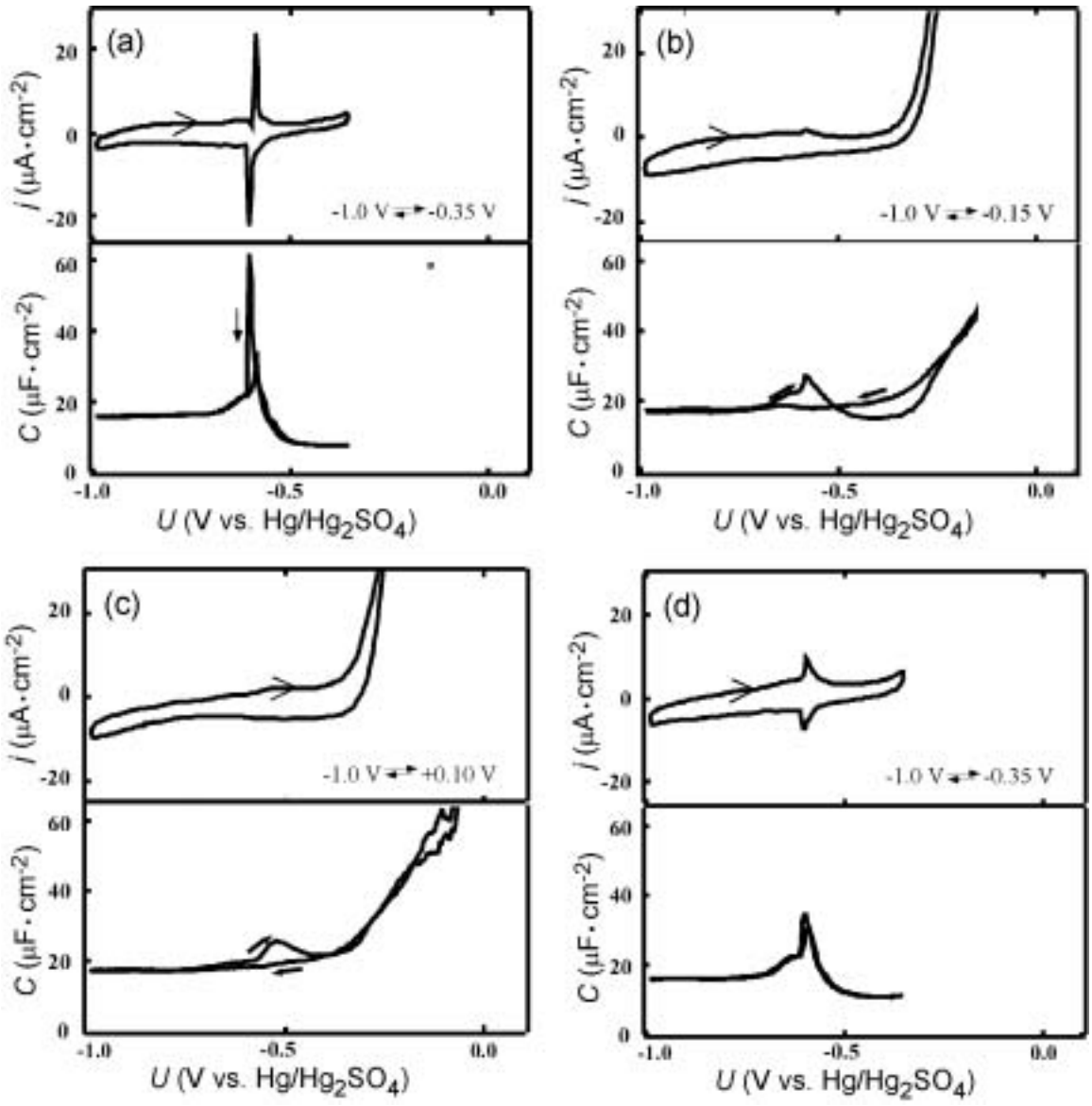

Figure 7.5: *Successive current– and capacitance–voltage measurements of the system Au(111)/5 mM camphor, 0.2 mM $K_4[Fe(CN)_6]$, 0.1 M $NaClO_4$ with various positive turning points, U_p: a) -0.35 V; b) -0.15 V; c) +0.10 V; d) -0.35 V. (Rotation frequency 29 rps, scan rate 50 mV/s).*

This slow time constant, with which the adsorption behavior of camphor is modified, can be seen better in Fig. 7.6, where five consecutive CVs that were obtained when setting the positive turning point from -0.4 V to -0.2 V (thin solid lines) are displayed. In this case, both hexacyanoferrate species were in the solution, and the electrode was not rotated. For comparison, the CVs of the

camphor free electrolyte (long-short dashed line) and the camphor containing electrolyte in the negative reference scan region (-1.0 V to -0.4 V) are also shown. Clearly, after setting U_p to -0.2 V, the phase transition peak decreases from scan to scan, whereas the reaction current gradually increases, although it has not yet reached the value of the camphor free system in the last scan shown. Furthermore, a peak at about -0.3 V develops.

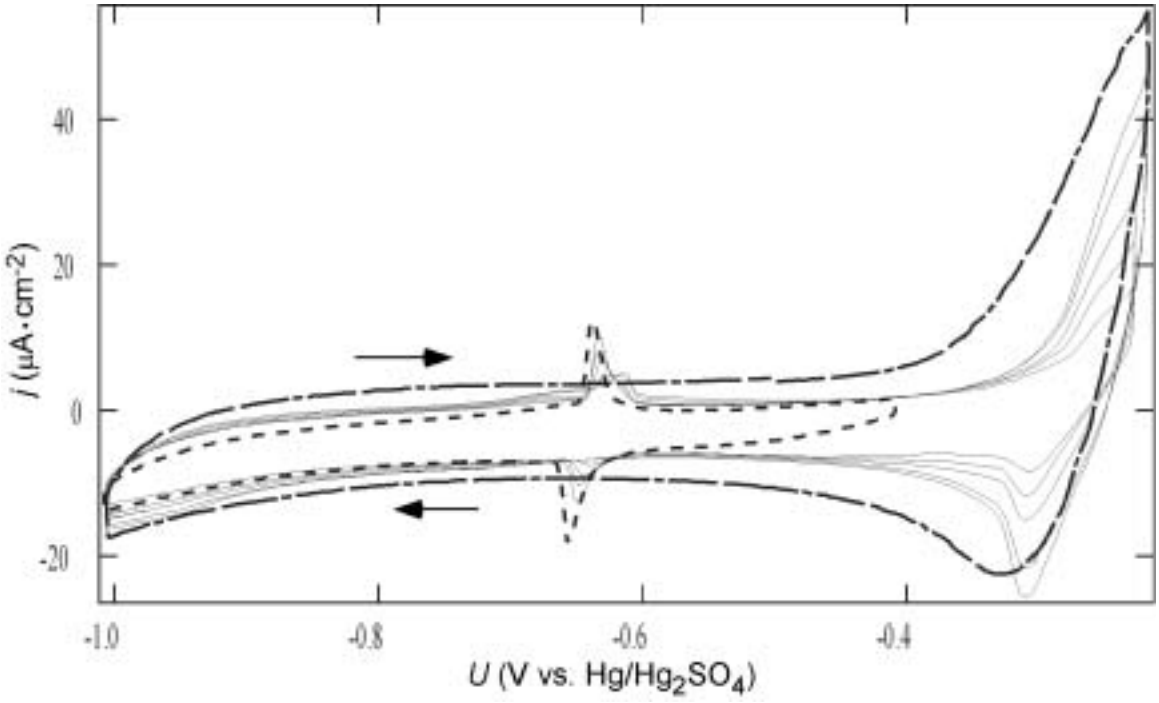

Figure 7.6: *Successive cyclic voltammograms in the potential range [-1 V, -0.2 V] of the system Au(111)/5 mM camphor, 0.2 mM $K_3[Fe(CN)_6]$, 0.2 mM $K_4[Fe(CN)_6]$, 0.1 M $NaClO_4$ (thin solid lines) in comparison with a cyclic voltammogram of the same system in a potential range [-1 V, -0.4 V] (dashed line), and of a system without camphor (long-short dashed line). (Stationary electrode; scan rate 50 mV/s).*

Discussion

The results from Figs. 7.5 and 7.6 suggest that at potentials positive to -0.2 V the electrode surface is irreversibly modified through an adsorbate, which does not reversibly desorb negative to -0.2V. Furthermore, as evident from Fig. 7.6, the adsorbate lifts the inhibition of the oxidation of $Fe(CN)_6^{4-}$ and the reduction of $Fe(CN)_6^{3-}$ by the condensed camphor film. This observation together with the

capacitance measurements (Fig. 7.5) point to the fact that the adsorbate displaces the adsorbed camphor molecules rather than that it adsorbs on top of the camphor layer.

Concerning the nature of the adsorbate, the most obvious candidate would be $Fe(CN)_6^{4-}$, or, since the displacement occurs at potentials, at which the oxidation sets in, the reaction product $Fe(CN)_6^{3-}$. However, one can expect that these anions would desorb reversibly, and thus neither the reduced amount of adsorbed camphor on the positive scans nor the slow and only partial recovery of the phase transition peaks appears to be consistent with this assumption. Rather, it is much more likely that polymeric hexacyanoferrate complexes form on the electrode. This conjecture was further investigated employing SPR measurements.

7.3.2 Surface plasmon resonance measurements on Au(111) film electrodes

Results and discussion

In Fig. 7.7 a sequence of CVs and SPR curves is displayed. The curves were obtained after adding $K_4Fe(CN)_6$ to the camphor containing electrolyte at a fixed potential of -0.8 V. Subsequently, the applied voltage was cycled between -0.9 V and -0.45 V for 15 minutes to allow a complete mixing of the electrolyte.

After the addition of ferrocyanide, the SP resonance angle shifted to slightly larger angles due to the changed dielectric constant of the electrolyte. Already after about 1 minute the SPR signal was constant. The resulting SPR angle voltage characteristic is curve 1 in Fig. 7.7b. As evident from both, the CV (see inset of Fig. 7.7a) and the SPR measurement, as long as the applied voltage is lower than -0.4 V, the phase transition remained essentially unaffected by the presence of ferrocyanide.

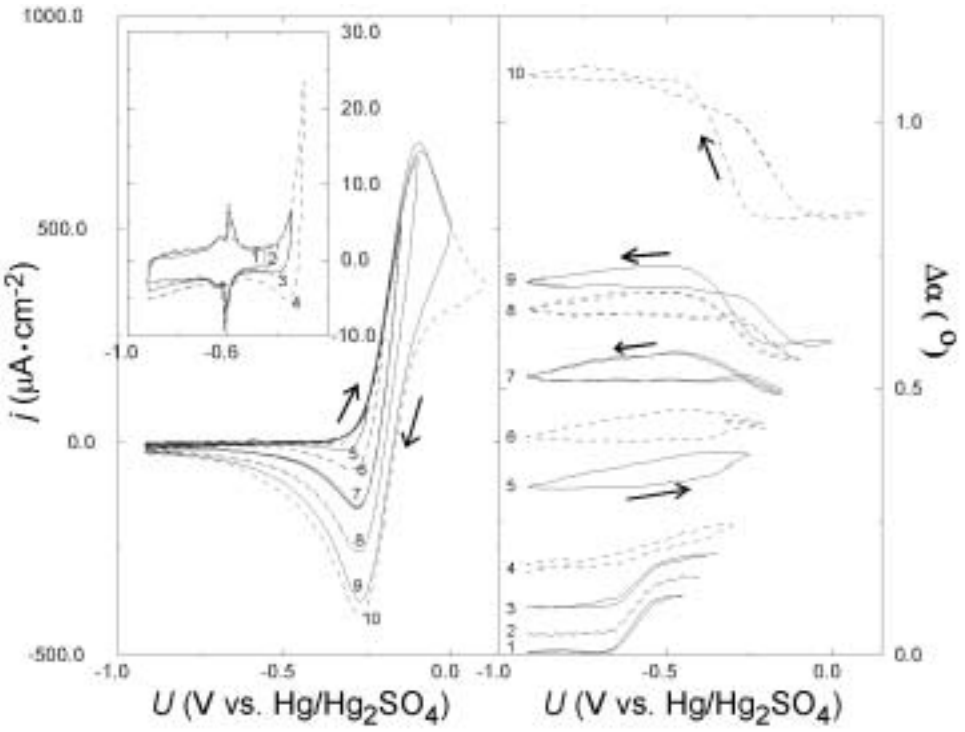

Figure 7.7: *Cyclic voltammograms (a) and simultaneously recorded SPR angle voltage curves (b) of a Au film electrode in 5 mM camphor, 5 mM $K_4[Fe(CN)_6]$, 0.1 M $NaClO_4$ for different positive turning points, U_p. U_p was increased in steps of 50 mV from -0.45 V on. (Scan rate 50 mV/s.)*

Curves 2 to 10 in Fig. 7.7 show how the SP resonance angle and the CV change when subsequently increasing the positive turning point in steps of 50 mV. At positive turning points of -0.4 and -0.35 V, the phase transition peak is still present in the CV, although its height is reduced (Fig. 7.7a, inset). In accordance with this observation, the SPR angle voltage curve still exhibits the step that indicates the formation of the camphor film, but its height is reduced compared to the curve 1. However, there is another striking feature of the SPR angle voltage curve: The entire curve is shifted towards larger angles. When cycling the potential for an extended time in these potential ranges, a stationary situation never establishes. Rather, the SPR curves continue to gradually shift toward more positive angles, which goes along with a decrease of the height of the PT peak in the CVs.

When setting the positive turning point to -0.3 V, the picture changes qualitatively: The PT peak disappears already after the first cycle, and the SPR

curve lacks the step that originates from the adsorption of camphor. Instead, it exhibits a hysteresis in the forward and backward scan with a nearly linear decrease of the angle shift with the potential in the negative scan. Again, with time a shift of the entire curve toward larger resonance angles is observed, the shift being faster than for curves 2 and 3. Setting the positive turning point to -0.25 V and -0.2 V, the difference in the two scan directions becomes more pronounced, and the angle shift of the entire curve with time becomes faster.

For values of U_p > -0.2 V a second hysteresis develops in the SPR angle curves. On the positive scan the resonance angle starts to decrease at about -0.25 V until it reaches a plateau at about -0.1 V. On the negative scan the SPR angle is constant until about -0.25 V, from where it starts to increase again. The more positive U_p, the more pronounced is the hysteresis in the potential range between -0.3 and -0.1 V, and the more drastic the shift of the entire SPR angle voltage curve toward more positive angles.

The CVs corresponding to the experiments with Up > -0.2 V approach a form characteristic for quasi-reversible redox reactions in stagnant solution. In contrast to the SPR angle voltage curves, these curves do not exhibit any sign of a continuous change of the electrode surface.

The continuous shift of the SPR angle voltage curves strongly supports the conjecture derived above from the single crystal experiments, namely that positive to a threshold potential the camphor film is gradually replaced by polymeric hexacyanoferrate complexes. These complexes can be regarded as a precursor of Prussian White-, resp. -Blue-type films which form at more positive potentials and after longer reaction times. The hysteresis in the SPR angle voltage curves at positive potentials (i.e., between -0.25 and -0.1 V) is due to the oxidation/reduction of Prussian White and Prussian Blue, respectively. The difference in the (complex) dielectric constants of these two film compositions gives rise to the observed drastic changes in the resonance angle (see, e.g., curve 10), the continuous shift in the resonance angle being due to the growth of the films. Obviously, the film formation is the faster, the more positive U_p is. Furthermore, the fact that the threshold potential is more negative for the film

electrode than in the case of the single crystal is in favor of the interpretation that the camphor layer is replaced by the hexacyanoferrate film.

7.4 Formation of a polymeric hexacyanoferrate adsorbate on the Au film electrode in the absence of camphor: SPRA measurements

Results and discussion

In order to investigate in how far the adsorbed camphor layer influences and possibly catalyzes the Prussian Blue-type film formation, we performed the same experiment in the camphor free electrolyte. Fig. 7.8a displays the obtained CVs and Fig. 7.8b the corresponding SPR angle voltage curves. Owing to the absence of camphor, the SPR angle voltage curves do not exhibit a step-like increase in the resonance angle at the potential, at which the phase transition occurs in the curves with the most negative turning points (curves 1 to 3). Except for this difference, the series of SPR angle voltage curves exhibits the same qualitative features as those in Fig. 7.7. In particular, first, a shift of the entire curve with time is observed, which is the faster, the more positive U_p is, and second, for $U_p >$ -0.25 V, a significant decrease of the resonance angle occurs at positive potentials and a pronounced hysteresis develops. The threshold potential of U_p, from which on the SPR angle curve starts to shift, is -0.45 V and thus more negative without camphor than with camphor. This indicates that camphor protects the Au surface at these negative potentials against the formation of polymeric hexacyanoferrate complexes on the electrode surface, which constitutes further evidence that camphor is replaced by the polymeric film rather than that the film forms on top of the condensed camphor layer.

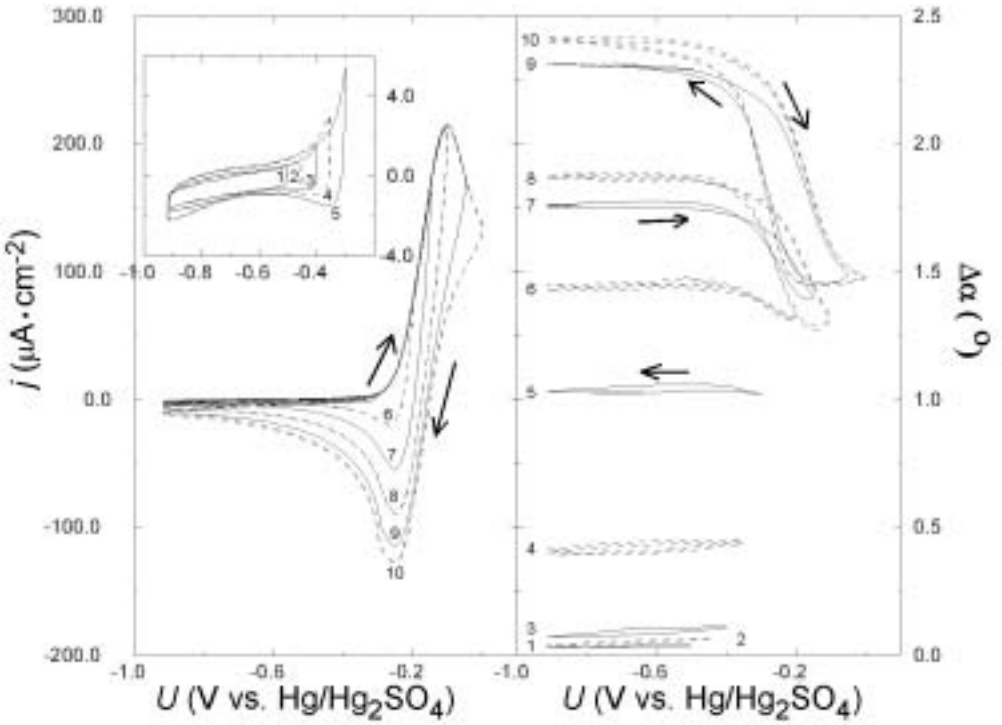

Figure 7.8: *Cyclic voltammograms (a) and simultaneously recorded SPR angle voltage curves (b) of a Au film electrode in 5 mM camphor, 5 mM $K_4[Fe(CN)_6]$, 0.1 M $NaClO_4$ for different positive turning points, U_p. U_p was increased in steps of 50 mV from -0.45 V on. (Scan rate 50 mV/s.)*

We should note that SPR angle measurements during the oxidation and reduction of $Fe(CN)_6^{4-/3-}$ on Au were also reported in [118]. In this study, the potential was cycled about 300 mV around the formal redox potential of the reaction. The authors observed SPR angle voltage curves that exhibited a hysteresis around the formal redox potential (similar to our curves at U_p > -0.2 V). They attribute the change in the resonance angle to a refractive index change within the diffusion layer due to changed ratios of the concentrations $Fe(CN)_6^{3-}$ and $Fe(CN)_6^{4-}$. This seems to be in contrast to our interpretations that from the beginning the dependence of the SPR signal is dominated by the formation of a surface film. Our measurements with camphor do not leave any doubt that some polymeric adsorbate covers the electrode surface even during the first potential cycle if $U_p > U_{th}$ (≈ -0.3 V for the film electrode and -0.2 V for the single crystal electrode), and this should also be the case under the conditions used in [118]. However, it might be that for 15 to 150 times larger concentration of $Fe(CN)_6^{4-/3-}$ as was used in [118], the change in the refractive index in the electrolyte close to the surface is large compared to the refractive index change due to the beginning

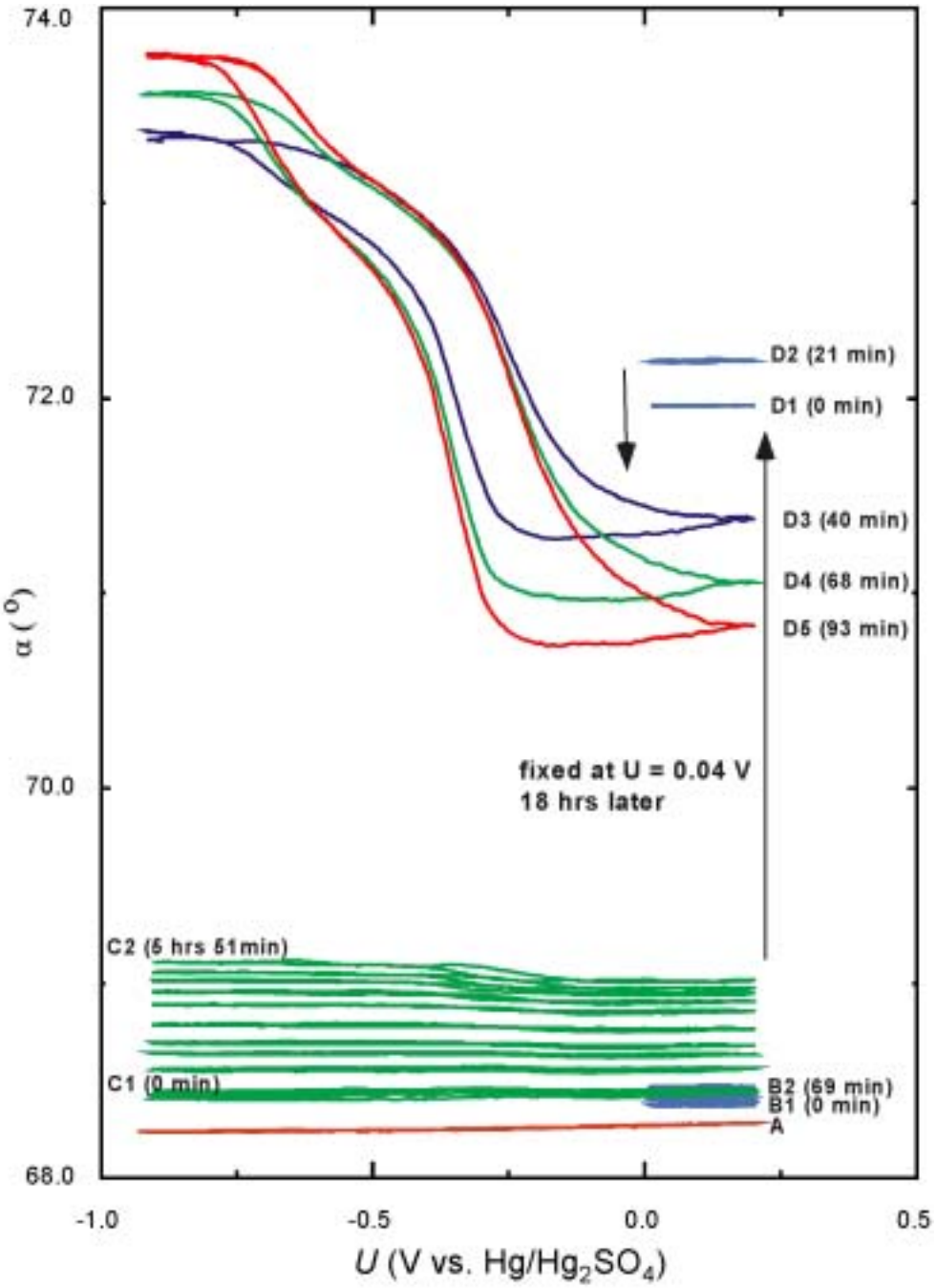

Figure 7.9: *Evolution of the SPR angle voltage curves in the system Au(111) film electrode/$Fe(CN)_6^{3-}$, ClO_4^-. In all curves the voltage was scanned with 50 mV/s. Curve A was obtained in the pure supporting electrolyte (0.1 M perchlorate). B1 to B2 are taken in the potential region 0.0 − 0.2 V after adding 5 mM $Fe(CN)_6^{3-}$ into the electrolyte. 69 minutes after adding ferricyanide the potential region was enlarged from -1.0 to +0.2 V, and C1 to C2 were recorded within the next 5 hours and 51 minutes. Subsequently the voltage was fixed at 0.04 V (where $i \approx 0$ mA) for 18 hours, then curves D1 to D2 (small potential region) and D3 to D5 (large scan region) were recorded.*

film formation, and thus the film formation could not be detected in the SPR angle voltage curve for short experimental times. There is ample experimental evidence in literature that Prussian Blue modified electrode surfaces can be formed electrochemically starting with a solution containing $Fe(CN)_6^{4-/3-}$ [109, 119-126]. However, in these studies much more drastic conditions are used, such as larger concentrations of hexacyanoferrate, Cl^- ion containing electrolytes, and, more importantly, more positive potentials and longer reaction times are applied. The novel insight into the $Fe(CN)_6^{4-/3-}$ redox reaction in this study is that even in neutral perchlorate solutions with only a low concentration of $Fe(CN)_6^{4-/3-}$ and at potentials about 150 mV negative to the formal redox potential, polymeric hexacyanoferrate complexes, which can be regarded as a precursor of the Prussian Blue-type film, adsorb on the electrode.

We conclude that it is impossible to study the electron transfer rate of $Fe(CN)_6^{4-}$ oxidation or $Fe(CN)_6^{3-}$ reduction at the bare Au/electrolyte interface, except for very negative potentials. Rather, around the equilibrium potential of the reaction, a Prussian Blue-type film always covers the electrode. Changes of the electrode surface, due to the formation of a polymeric hexacyanoferrate film, occur already on a time scale that is short compared to the time, in which a typical CV is recorded. Furthermore, the interaction between the polymeric adsorbate and the Au electrode is so strong that condensed organic films may be replaced.

To further characterize the Prussian Blue-type film formation, long-time SPR studies were carried out. They were done by adding only $Fe(CN)_6^{4-}$ to the supporting electrolyte as in the experiments discussed above as well as by adding only $Fe(CN)_6^{3-}$. When adding only the oxidized species, initially the potential region was restricted to positive values, at which the $Fe(CN)_6^{3-}$ reduction rate was negligible. In this way it was possible to test, whether in the positive potential region a film also forms in the presence of just one rather than both oxidation states of hexacyanoferrate. Such a long-term measurement is displayed in Fig. 7.9. Curve A in Fig. 7.9 was obtained with the base electrolyte (0.1 M $NaIO_4$). When adding $Fe(CN)_6^{3-}$ to the electrolyte, the SPR angle shifted to a larger value, as it was the case when we added the reduced species. This initial fast shift can be attributed to the change in refractive index of the electrolyte

upon introduction of the $Fe(CN)_6^{3-}$. After addition of ferricyanide, the voltage was initially cycled between 0.2 and 0 V vs. Hg/Hg_2SO_4. Within this potential region the reduction current was negligible. Still apparently, from the shift of curve B1 to curve B2, the resonance minimum slightly shifted towards more positive potential values. This shift was considerably larger than the negligible one we observed when cycling the reduced species in a negative potential region (see above). Hence, we conclude that even in the absence of the reaction a film forms on the electrode surface in the positive potential region. The stronger tendency of the ferrocyanide ion as opposed to the ferricyanide ion to form a film might be related to its lower stability. It partially dissociates according to:

$$Fe^{III}(CN)_6^{3-} \leftrightarrow Fe^{III}(CN)_3 + 3CN^-.$$

It seems to be likely that the neutral $Fe^{III}(CN)_3$ molecules adsorb and consecutively polymerize on the electrode [110, 111, 127, 128].

When setting the negative turning point to -1.0 V, i.e., cycling across the reversible redox potential, the same development of the SPR angle voltage curves is seen when starting with $Fe(CN)_6^{4-}$. The entire curve shifts continuously to larger values, and a hysteresis starts to develop (curves C1 to C2 in Fig. 7.9). Fixing the voltage at 0.04 V for 18 hours and cycling subsequently again in the restricted and full potential ranges leads to the curves from D1 to D5 in Fig. 7.9. Clearly, dramatic changes occurred in both, the offset of the entire curves and, even more impressively, the amplitude of the hysteresis, which now amounts to nearly 3°. Furthermore, the hysteresis in the SPR angle voltage curves does not involve just two, but three levels. This is a hint that the hexacyanoferrate film undergoes two consecutive oxidation -, respectively reduction steps. When these pronounced changes occurred in the SPR, also the cyclic voltammogram exhibited some new features. As can be seen in Fig. 7.10, there is a small peak superimposed on the reduction wave, and a peak pair is recognizable, centered around about -0.65 V, with a separation of the maxima of about 100 mV. It is tempting to conclude that the two peaks in the negative scan are associated with the two steps in the SPR angle voltage curve. On the anodic scan there is only one additional peak recognizable. As the redox wave stemming from the

$Fe(CN)_6^{3-}/Fe(CN)_6^{4-}$ reduction, respectively oxidation, is by far larger than the peaks that might be associated with oxidation and reduction processes of the adsorbed films, it is conceivable that the second peak is hidden by the oxidation wave.

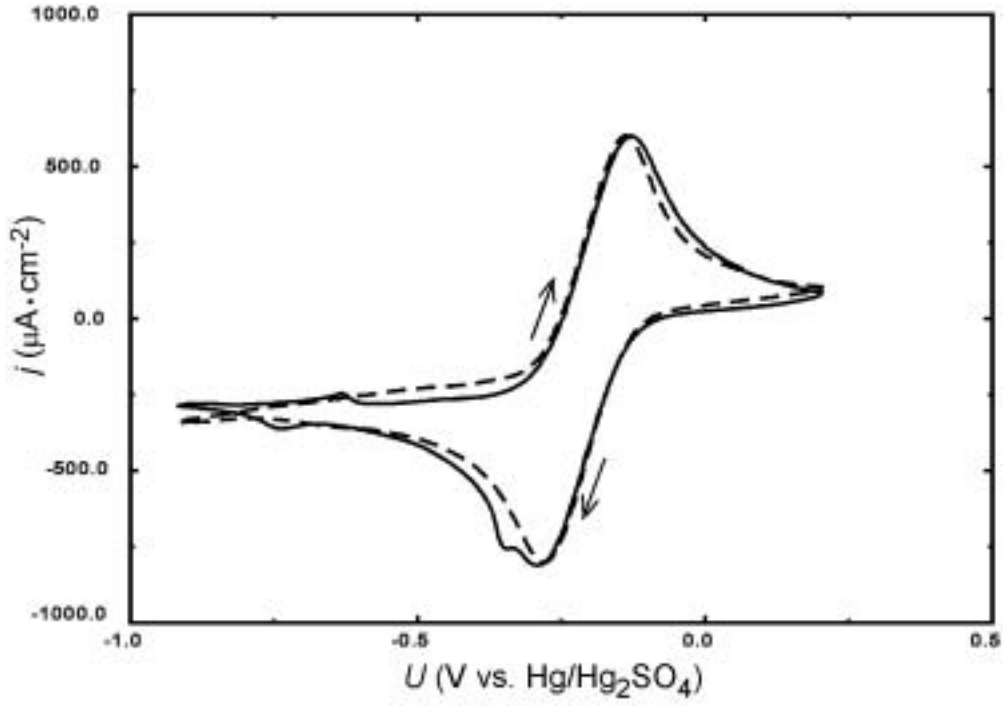

Figure 7.10: *Cyclic voltammograms of the Au(111) film electrode in 5 mM $Fe(CN)_6^{3-}$ and 0.1 M $NaClO_4$, scan rate, 50 mV/s. Dashed line: CV at the beginning of the experiment; solid line: final CV (after one day).*

To further investigate the correlation between oxidation and reduction of the adsorbed film and the SPR angle shift, the hexacyanoferrate containing electrolyte was carefully exchanged by a pure $NaClO_4$ electrolyte without touching the electrochemical cell or the optical devices. The I/U and SPR angle/U curves obtained in the pure base electrolyte are reproduced in Fig. 7.11. Surprisingly, neither the cyclic voltammogram exhibits current peaks at those positions, at which they occurred in the hexacyanoferrate containing solution after a long cycling time, nor the SPR angle voltage curves exhibit two steps.

Instead, the SPR curves possess two levels that lie ca. 3° apart and are smoothly connected over a potential interval of roughly 250 mV. The curves do not exhibit a hysteresis between the positive and negative scans.

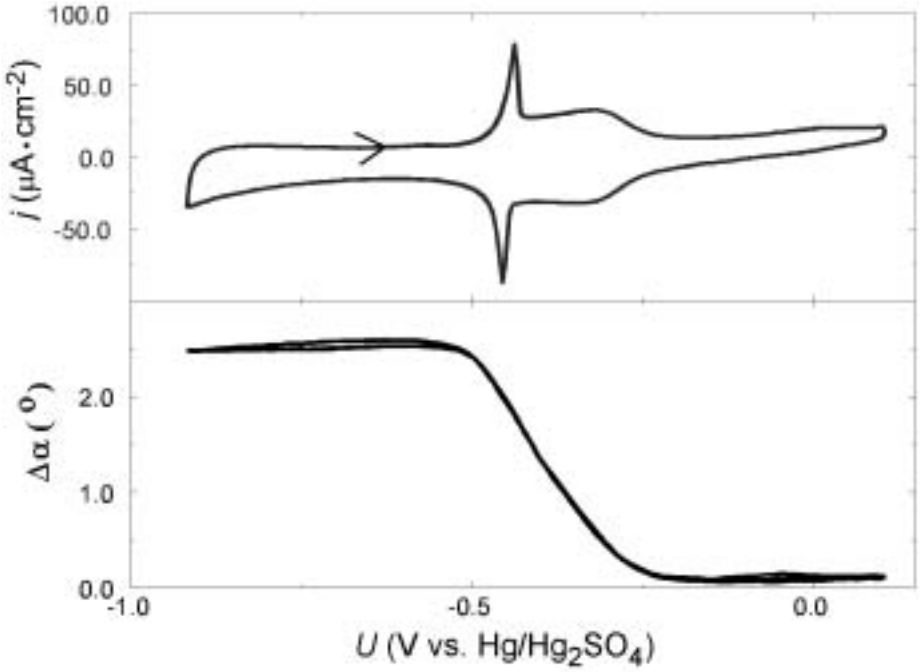

Figure 7.11: *Cyclic voltammogram (top) and simultaneously recorded SPR angle voltage curve (bottom) of the Au(111) film electrode modified by a film that had been formed when cycling the electrode in a hexacyanoferrate containing electrolyte reaction after exchanging the electrolyte to 0.1 M $NaClO_4$ (Scan rate, 50 mV/s).*

Also the cyclic voltammogram can be viewed as being composed of three regions. Approximately, the positive third and the negative third of the CV exhibit typical double layer charging behavior. These regions correspond to the regions, in which also the SPR angle is independent of the applied potential. Between these regions, and thus in the region in which the SPR changes drastically, also the current density is considerably higher. In a small potential interval at the negative end of this region, there is a sharp peak pair on top of this enhanced current level. The combination of CV and SPR measurement strongly support the conclusion that the change in SPR is due to the oxidation, respectively reduction of the film, the most likely states involved being Prussian White (PW), which

exists at negative potentials, and Prussian Blue (PB), which is stable in the positive potential region of the experiment:

$$KFe^{III}[Fe^{II}(CN)_6] + e^- + K^+ \leftrightarrow K_2Fe^{II}[Fe^{II}(CN)_6] \quad (PB \leftrightarrow PW).$$

The sharp peak pair reminds of a typical phase transition peak. This fact as well as the fact that it is not associated with any visible change in the SPR angle support the interpretation that the peak pair stems from a change of the order of the film or the position of some atoms when cycling between the two forms of the film.

7.5 Summary

The phase transition peaks in the CV of camphor on Au(111) proved to be a sensitive probe for the interaction between the two-dimensional physisorbed film and a redox couple. CVs and capacitance measurements of the Au(111)/camphor, $Fe(CN)_6^{3-(4-)}$, ClO_4^- system revealed that camphor inhibits the reaction, as long as the electrode potential is more negative than 0.2 V vs. Hg/Hg_2SO_4, the decrease in the reaction rate being more pronounced in electrolytes of low ionic strength (0.1 M and 0.02 M) than in those of high ionic strength (0.8 M).

As soon as this threshold is exceeded, adsorption of a polymeric hexacyanoferrate film causes the destruction of the camphor film. Surface plasmon resonance measurements allowed to detect the initial adsorption of the hexacyanoferrate complexes in the submonolayer region and to follow their transformation to Prussian White, respectively, Prussian Blue films at longer reaction times and more positive potentials. Furthermore, it could be shown that also in the absence of camphor the Au electrode is covered by polymeric hexacyanoferrate compounds, once the electrode potential is positive to a threshold potential ($Fe(CN)_6^{4-}$). This potential is lower in the absence of the camphor film than in its presence.

The strong tendency of $Fe(CN)_6^{3-(4-)}$ to form polymeric adsorbates, which turn into Prussian White/Blue films at longer deposition times, even at the low

concentrations of $Fe(CN)_6^{3-(4-)}$ used in these studies, in neutral sodium perchlorate solution and at comparatively negative potentials, indicates that much care should be taken when using the $Fe(CN)_6^{3-}/Fe(CN)_6^{4-}$ charge transfer reaction as a benchmark system to characterize organic films on electrode surfaces or new electrode materials.